

A nonlinear numerical model for sloped-bottom tuned liquid dampers

D. E. Olson and D. A. Reed*

Department of Civil and Environmental Engineering, University of Washington, Campus Box 352700 Seattle, WA 98195-2700, U.S.A.

SUMMARY

Shaking-table data for a tuned liquid damper with a sloped bottom of 30° with the horizontal are investigated using a non-linear numerical model previously developed by Yu, Jin-kyu, Nonlinear characteristics of tuned liquid dampers. *Ph.D. Thesis*, Department of Civil Engineering, University of Washington, Seattle, WA, 98195 (1997). Stiffness and damping parameters for this model are obtained and compared with those previously derived for box-shaped tanks. The values for these parameters reflect the softening spring behaviour of the sloped-bottom system in contrast to the hardening system evident for the box-shaped TLD. Consequently, the sloped-bottom tank should be tuned slightly higher than the fundamental structural frequency in order to obtain the most effective damping. Copyright © 2001 John Wiley & Sons, Ltd.

KEY WORDS: structural control; fluid mechanics; structural dynamics

INTRODUCTION

The sloped-bottom tuned liquid damper has been investigated recently by Gardarsson [1] and Gardarsson *et al.* [2]. Its behaviour is markedly different from the more familiar box-shaped TLD whose bottom is flat. The box-shaped tank is a stiffness-hardening system; and unfortunately, it displays a beating property, when the force excitation has ceased; e.g., Reference [3]. Typically, baffles or floating particles are used in practice to alleviate this difficulty [4–7]. The motivation for the use of the sloped-bottom tank came from a desire to reduce or if possible prevent the phenomenon of beating. It is well-known in tsunami research that wave energy may be dramatically dissipated by the shores of an ocean coastline. In theory, adding a sloped bottom to a tank would provide the same dissipative property as a beach. Gardarsson [1] performed shaking-table tests on four cases using a sloped-bottom tank with an angle of 30° with the horizontal in order to examine this theory. Although he found that the characteristics of wave motion are different from the box-shaped tank, he was not able to conclusively

*Correspondence to: D. A. Reed, Department of Civil and Environmental Engineering, University of Washington, Campus Box 352700, Seattle, WA 98195-2700, U.S.A.

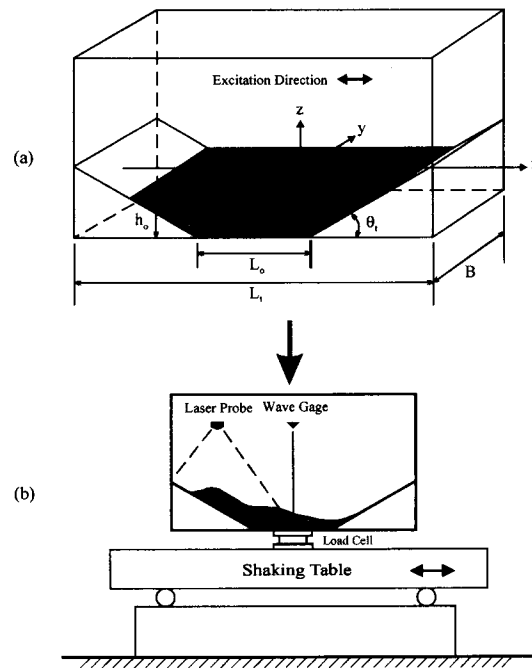


Figure 1. (a) TLD tank configuration using the wetted perimeter L_1 where $L_1 = L_0 + 2h_0/\sin(\theta_t)$; (b) shaking table experimental set-up.

evaluate the mitigation of the beating phenomenon, nor did he examine the data thoroughly for structural engineering applications.

The objective of this paper is to evaluate the sloped-bottom tank data in a structural engineering context. First, general characteristics of the wave motion in contrast to the box-shaped tank are discussed. Second, the parameters of the non-linear model developed by Yu [8] will be presented and discussed. The results of this analysis provide valuable information regarding the appropriate tuning and practical application of the sloped-bottom tanks. It is emphasized that the single tank itself is under investigation; for mitigation of vibration over a wide range of frequencies, multiple tanks tuned to different frequencies would have to be employed.

EXPERIMENTAL RESULTS

Figure 1 shows the experimental set-up used by Gardarsson [1] in measuring the data for the sloped-bottom tank. The experiments were performed using the shaking-table facility located at the University of Southern California. This table sits on a 1.2 m square platform weighing 350 kg that is anchored to a concrete floor. The table moves in a single direction horizontally through a hydraulic servo-control system. The test TLD was mounted on a load cell bolted onto the shaking table. The model is comprised of 1.27 cm thick Plexiglas plates with the exception of the bottom one being 1.9 cm to ensure rigidity. The sloped-bottom angle of 30° was the only sloped case examined. Because there was no special treatment to the sloped Plexiglas

Table I. Test data for tank with total base length $L_t = 590$ mm and width $B = 335$ mm.

Test case	Water depth h_0 (mm)	Empirically derived natural frequency f_w (Hz)	Excitation amplitude A (mm)
S590h40a025	40	1.28	2.5
S590h40a05	40	1.28	5
S590h70a025	70	1.06	2.5
S590h100a025	100	0.94	2.5

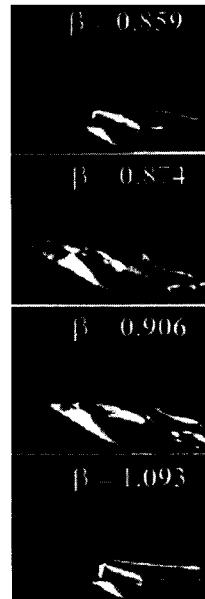


Figure 2. Video capture of the tank sloshing for amplitude $A = 5$ mm at selected frequency ratios. From top to bottom: Figures (a)–(d).

pieces, they were considered to be hydraulically smooth. Table I contains information on the tank dimensions and the water depth h_0 .

Capacitance gauges made from tantalum rods were used to measure the wave characteristics. More details of this equipment can be found in Reference [1]. In order to examine the temporal and spatial variations of the water-surface response, laser-induced fluorescent imagery was used. Illuminated images were captured by video camera, and a fast shutter speed of $1/250$ s was used to freeze the fast moving wave actions. Examples of the wave behaviour are given in the captured video images of one-half of the tank as shown in Figures 2(a) to (d). Figures 2(a) and 2(d) provide illustrations of small wave heights at very low- and high-frequency ratios, respectively. The frequency ratio β is defined as the ratio of the excitation frequency of the shaking table to the tank natural frequency. Figure 2(b) shows strong wave behaviour at a frequency ratio β between the two extremes shown in Figures 2(a) and 2(c), close to but less than unity. In Figure 2(b), it is noted that almost all of the water mass has travelled up the sloped portion of the tank with little temporal

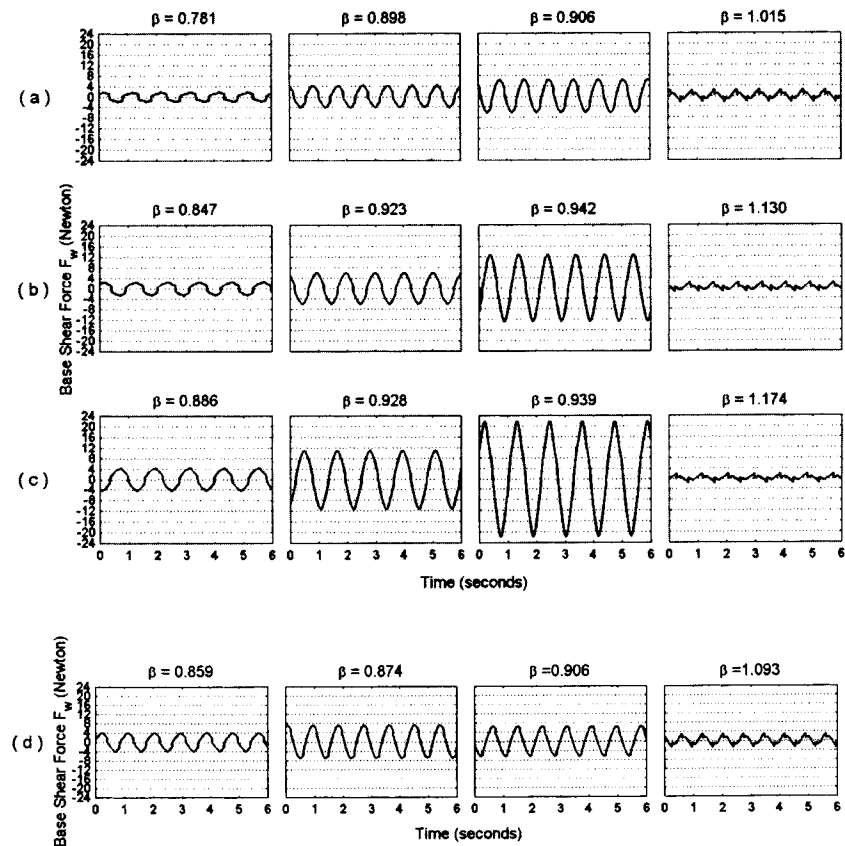


Figure 3. Time histories of the base shear force for the sloped tank at selected frequency ratios.

variation in the depressed water surface at the tank centre. Figure 2(b) is a video capture of the 'jump' phenomenon. Under base excitation, all TLD tanks exhibit a response that increases up to a particular frequency and then dramatically drops; this behaviour is called the 'jump' (e.g., Reference [3]). Because the sloped TLD response increases until a jump frequency ratio that is less than unity and then suddenly ceases, it is a softening spring system. In contrast, the box shape is a hardening spring system where the jump occurs at $\beta > 1$.

From a fluid mechanics perspective, it is interesting to note that the time history of the base shear force generated by the wave motion in the tank changes significantly with excitation frequency. Figures 3(a) to (d) show time series of the base shear force in Newtons at pre-jump, jump and post-jump excitation frequency ratios. These plots illustrate that the amplitude and the frequency content of the force undergo a significant transformation from the jump to post-jump frequencies. Also, although the magnitude of the amplitudes of the pre-jump and post-jump forces are comparable, their frequency content is very different, clearly indicating a different wave phenomenon in the post-jump region.

Estimation of the natural frequency of water sloshing in a sloped-bottom tank is not straightforward. In contrast, the linear natural frequency for the box shape can be evaluated using the

Table II. Comparison of natural frequency estimates.

Test case	Length L_1 (mm) from Equation (2)	Equation (1) using L_1	Empirically derived frequency [1] (Hz)	Percent difference
S590h40a025	250	1.20	1.28	-6.0
S590h40a05	250	1.20	1.28	-6.0
S590h70a025	370	1.06	1.06	0.0
S590h100a025	490	0.95	0.94	+1.0

dispersion relation [9] as follows:

$$f_w = \frac{1}{2} \sqrt{\frac{g}{\pi L} \tanh\left(\frac{\pi h_0}{L}\right)} \quad (1)$$

where f_w is the frequency in Hertz, g is the acceleration due to gravity, h_0 is the water depth and L is the tank length. Because of the sloped bottom, choosing a value to employ for L is not obvious. Gardarsson [1] evaluated the frequencies of the sloped-bottom tanks experimentally. These values were compared with an estimate from Lamb's equation above. The best fit was provided by the wetted perimeter L_1 as defined by

$$L_1 = L_0 + \frac{2h_0}{\sin \theta_t} \quad (2)$$

where all parameters are shown in Figure 1. Using the length L_1 in equation (2) resulted in a fairly close estimate as shown in Table II. Because this equation is undefined for values of $\sin \theta_t = 0$ its use is limited.

THE NON-LINEAR STIFFNESS AND DAMPING (NSD) MODEL

Many phenomenological models have been suggested for box-shaped TLDs; e.g., References [5, 8, 10–16]. Although the model developed by Sun *et al.* [14] uses a variable mass, the effective mass is 100 per cent for large-amplitude excitation. Yu [8] and Yu *et al.* [16] use variable non-linear stiffness and damping for their equivalent tuned mass damper (TMD) model, called the NSD model, while holding the mass constant. Yalla and Kareem [15] impose a slamming impact model in conjunction with an equivalent TMD. All of these models have been used to capture the base shear force generated by box-shaped tanks. Our objective in this paper is to evaluate the parameters using Yu's model, which employs an energy dissipation matching scheme to identify stiffness and damping parameters with a constant water mass. Derivation of the sloped-bottom parameters of this simple model will illustrate differences with the box-shaped tank and suggest trends for cases not yet evaluated experimentally. A more comprehensive analysis of the shallow water sloshing behaviour in the tank can be found in References [1, 2].

Figure 3 provides an illustration of the non-linear-stiffness-damping (NSD) models as a single-degree-of-freedom (SDOF) system with stiffness and damping parameters, k_d and c_d ,

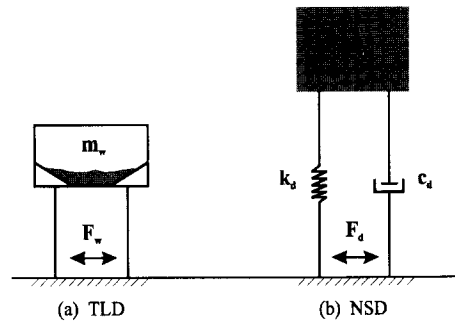


Figure 4. Schematic of TLD with base shear force F_w modelled as an equivalent NSD with damping force F_d , stiffness k_d , and damping c_d parameters.

respectively. These parameters are determined such that the energy dissipation provided by the NSD is equivalent to that of the TLD. The design challenge is to transform the appropriate parameter set derived for the equivalent solid mass damper into the liquid damper system. The mechanical model of TLD used for numerical simulation is based upon the development of a control force created by the sloshing motion of the liquid in the tank. In treating the TLD as an equivalent linear system, this force will be characterized by its amplitude and phase. Therefore, the matching scheme must incorporate the combined effect of these two properties. The single parameter of energy dissipation per cycle E_d is used to match this combination as by definition it is the area inside the loop of the control force vs the tank base displacement contour.

Figure 4 presents a typical sweep frequency plot of the non-dimensional energy dissipation per cycle for the sloped-bottom TLD with water depth $h_0 = 70$ mm and excitation amplitude $A = 2.5$ mm and for its corresponding NSD model. The softening spring behaviour is clearly evident as the dissipation peaks at $\beta < 1$. The non-dimensional energy dissipation curve for the TLD, E'_w (solid line) is determined from measurements of the shaking-table experiments. It is defined as

$$E'_w = \frac{E_w}{\frac{1}{2}m_w(\omega A)^2} \quad (3)$$

where m_w is the mass of the liquid; ω is the excitation angular frequency of the shaking table; A is the amplitude of the sinusoidal excitation; and the denominator of Equation (3) is the maximum kinetic energy of the water mass treated as a solid mass. The numerator is the energy dissipation per cycle as defined as

$$E_w = \int_{T_s} F_w dx \quad (4)$$

with dx referring to integration over the shaking-table displacement per cycles, and F_w the force generated by the liquid sloshing motion in the tank.

Table III. Summary of sloshing characteristics.

A (mm)	h_0 (mm)	β_{jump}	κ	ζ_d
2.5	40	0.91	0.83	0.018
2.5	70	0.94	0.89	0.017
2.5	100	0.95	0.88	0.012
5	40	0.87	0.78	0.024

The expression for the non-dimensional energy dissipation for the corresponding NSD model E'_d (dashed lines) is determined from the analysis of its behaviour, when subjected to harmonic base excitation. Details of this process may be found in Reference [16]. The parameters of primary interest are defined below:

β is the excitation frequency ratio defined by $\beta = f_e/f_d$;
 f_e is the excitation frequency;
 f_d is the natural frequency of the NSD model defined by $f_d = (1/2\pi)\sqrt{k_d/m_d}$;
 ζ_d is the damping ratio of the NSD model defined as $\zeta_d = (c_d/c_{cr})$;
 c_{cr} is the critical damping coefficient defined by $c_{cr} = 2m_d\omega_d$;
 ω_d is the linear fundamental natural angular frequency defined as $\omega_d = 2\pi f_d$;
 m_d, k_d and c_d are the mass, stiffness and damping coefficients of the NSD model, respectively.

The non-dimensional energy dissipation for the NSD model at each excitation frequency is obtained numerically and fit by the least-squares method over the frequency range of high-energy dissipation. In this scheme,

$$m_d = m_w$$

Beginning with initial estimates of ζ_d and f_d the scheme determines values of the stiffness and damping coefficients for the experimental cases outlined in Table I. In analysing the results, it is useful to evaluate the stiffness changes through two ratios. The first is the frequency shift ratio ξ , defined as

$$\xi = \frac{f_d}{f_w} \quad (5)$$

in which f_w is the linear fundamental natural frequency from Equation (1). Second, the stiffness hardening ratio κ is defined as

$$\kappa = \frac{\kappa_d}{\kappa_w} \quad (6)$$

in which $\kappa_w = m_w(2\pi f_w)^2$. Because $m_d = m_w$,

$$\kappa = \xi^2 \quad (7)$$

The matching scheme provided the following values of κ and ζ_d as tabulated in Table III. The jump frequency ratio β_{jump} is also provided to indicate the degree to which

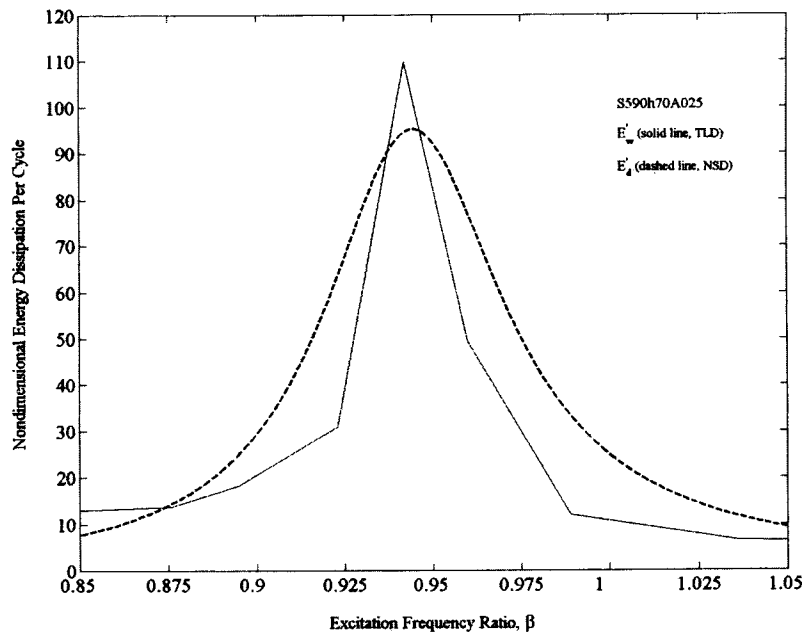


Figure 5. Comparison of non-dimensional energy dissipation.

softening behaviour occurs. The tank experiences greater softening at the larger excitation amplitude.

Previous work by Yu illustrated the dramatic change in stiffness with the advent of strong wave breaking for box-shaped tanks, as well as relationships for the damping and stiffness as a function of the non-dimensionalized excitation amplitude as defined by A/L . Obviously, the choice of ' L ' in this equation becomes cumbersome in the sloped analysis. Therefore, the ratio of A to the cubic root of the volume of water, V_w , in the tank was employed, $A' = A/\sqrt[3]{V_w}$. The limited sloped-bottom data only allowed for development of a best-fit relationship in the range $0.01 \leq A' \leq 0.05$, whereas sufficient box-shaped data allowed equations to be developed in the full range up to $A' = 0.30$. Jump frequency ratio values appear to be represented only slightly better using the new ratio $A' = A/V_w^{1/3}$ compared to the previous ratio A/L used by Yu [8]. In Figure 5, two types of trend lines are given for the box-shaped data and one trend line given for the sloped-bottom data. For the slope data in Figure 6, a 'linear' relationship represents the limited among of data very well having a value of $R^2 = 0.919$ for the best-fit equation. The best-fit equation is given below for the limited data set:

$$\beta_{\text{jump}} = 0.705 \times (A')^{-0.066} \quad \text{for } 0.01 \leq A' \leq 0.05 \text{ (linear)} \quad (8)$$

For the box data in Figure 6, a 'bilinear' relationship is represented by the dashed line and a 'linear' relationship by the solid line. Best-fit equations are given below for the linear and

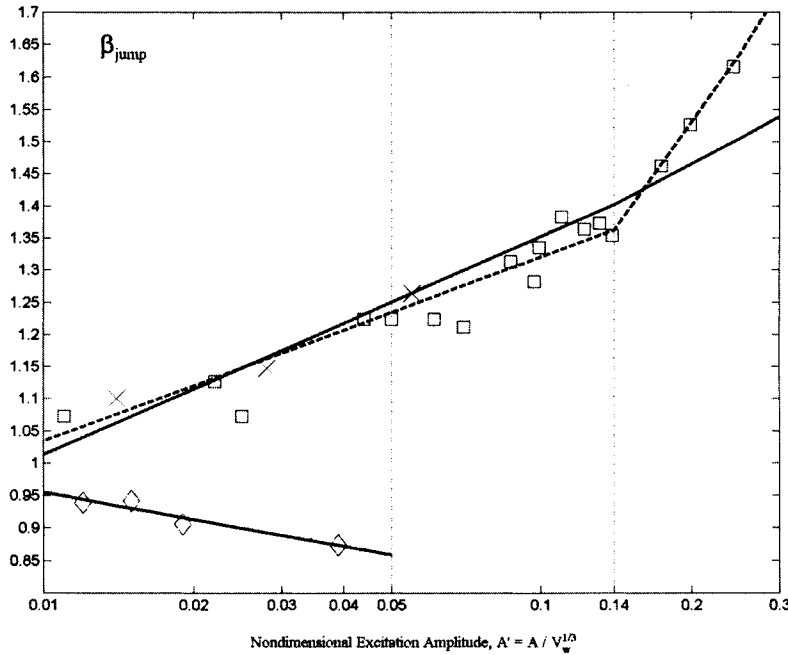


Figure 6. Jump frequency ratio β_{jump} plot for tank data in Table 3.4 using the symbols: (X) for box data from Sun *et al.* (1992); for box data from Yu (1997); and (\diamond) for slope data. For box data: solid line (linear), dashed line (bilinear).

bilinear curves of the box-data set:

$$\beta_{jump} = 1.785 \times (A')^{0.12} \quad \text{for } 0.01 \leq A' \leq 0.30 \quad (\text{linear}) \quad (9)$$

$$\beta_{jump} = \begin{cases} 1.677 \times (A')^{0.105} & \text{for } 0.01 \leq A' \leq 0.14 \\ 2.541 \times (A')^{0.318} & \text{for } 0.14 \leq A' \leq 0.30 \end{cases} \quad (\text{bilinear}) \quad (10)$$

Both trend lines match the jump frequency ratios very well up to $A' = 0.14$, but above this value, non-linear effects appear to be more influential and the linear curve underestimates the jump frequency ratio values. However, the linear relationship does provide a simpler correlation to the overall box data up to $A' = 0.30$. The R^2 values are 0.910 and 0.998 for the bilinear curve, before and after the break point $A' = 0.14$, respectively; the linear curve has a value of $R^2 = 0.906$ over the entire range. Even though a linear curve is simpler to use than a bilinear curve, future data points at values $A' > 0.30$ may require using a bilinear curve because a linear curve does not capture the non-linear influence and greatly underestimates jump frequency values.

Figure 7 plots the damping ratio values for the sloped-bottom and box-shaped tanks using the updated non-dimensional excitation amplitude ratio A' . For the slope data, a 'linear' relationship

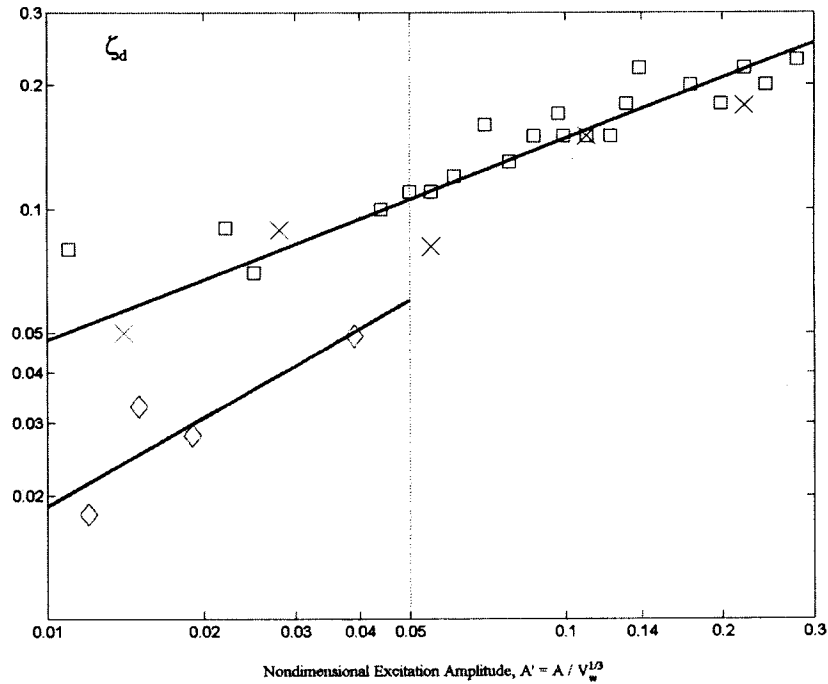


Figure 7. Damping ratio ζ_d plot for tank data using the symbols: (X) for box data from Sun *et al.* (1995); for box data from Yu (1997); and (\diamond) for sloped TLD data.

represents the data moderately well having a value of $R^2 = 0.790$. The best-fit equation is given below:

$$\zeta_d = 0.520 \times (A')^{0.721} \quad \text{for } 0.01 \leq A' \leq 0.05 \quad (\text{linear}) \quad (11)$$

The damping ratio values for the sloped-bottom tank clearly increase with an increase in the excitation amplitude ratio A' . The data values are much lower than the box data and also may slightly level off at higher excitation amplitudes, however more extensive data are needed to verify this trend. The damping ratio trends seem equally represented using either the new ratio A' or the previous A/L ratio from Yu [8].

For the box data in Figure 7, a 'linear' relationship is used to represent the box data, including data from Reference [14]. The best-fit equation has a value of $R^2 = 0.868$ and is given below:

$$\zeta_d = 0.456 \times (A')^{0.489} \quad \text{for } 0.01 \leq A' \leq 0.30 \quad (\text{linear}) \quad (12)$$

Figure 8 shows the stiffness hardening ratio values. For the sloped data, the best-fit equation presented below has an $R^2 = 0.925$:

$$\kappa = 0.527 \times (A')^{-0.120} \quad \text{for } 0.01 \leq A' \leq 0.05 \quad (\text{linear}) \quad (13)$$

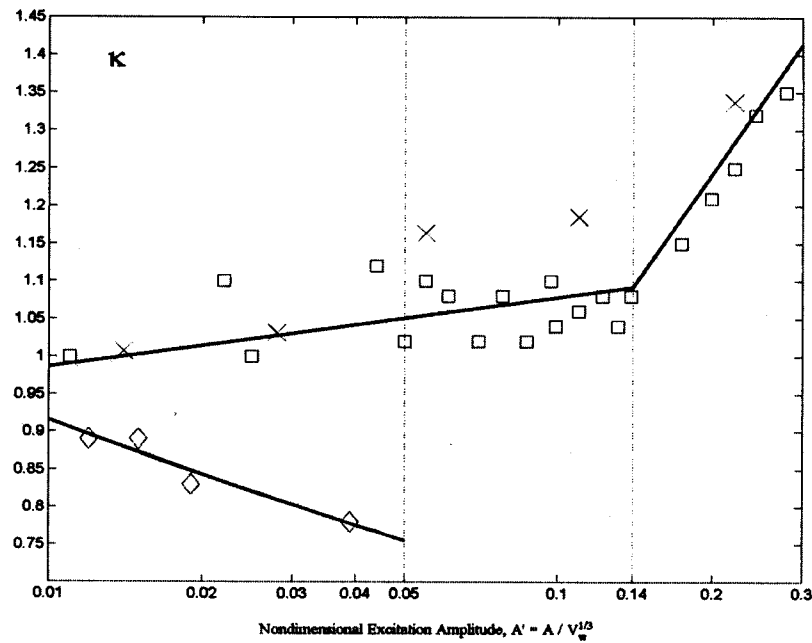


Figure 8. Stiffness ratio κ plot for tank data using the symbols: (X) for box data from Sun *et al.* (1995); for box data from Yu (1997); and (\diamond) for sloped TLD data.

The negative sloping curve for the slope data is related to the softening spring system for similar reasons to the jump frequency ratio trends. The stiffness hardening ratio values decrease with an increase in the A' values as the water depth decreases for a constant excitation amplitude A .

For the box data in Figure 8, a 'bilinear' relationship is used to represent the box data, including data from Reference [14]. The R^2 values are 0.364 and 0.912 for the bilinear curve, before and after the break point $A' = 0.14$, respectively. A 'bilinear' relationship appears most appropriate for the box-data stiffness values even though considerable scatter is evident by the value of $R^2 = 0.364$ in the region $A' < 0.14$. The higher stiffness values from Reference [14] can be partly attributed to rounding errors after converting the plotted data values from Reference [14] into an equivalent form used in the current NSD model. The best-fit equations are given below.

$$\kappa = \begin{cases} 1.197 \times (A')^{0.042} & \text{for } 0.01 \leq A' \leq 0.14 \\ 2.160 \times (A')^{0.352} & \text{for } 0.14 < A' \leq 0.30 \end{cases} \quad (\text{bilinear}) \quad (14)$$

Correlation is much better for the second part of the bilinear curve at values of $A' > 0.14$. The second part clearly shows a presence of non-linear behaviour that significantly increases the stiffness hardening ratio values. Both trend lines relate to a hardening spring system having increased stiffness hardening ratios with respect to the A' ratio (Figure 8).

DISCUSSION

The results given here for the sloped bottom tank have implications for structural control applications.

- From Figure 2(b), it is apparent that almost the entire water mass is involved in sloshing near the jump frequency. The sloped bottom makes more efficient use of the system mass during force excitation than the comparable box shape.
- Initial tuning of the sloped-bottom tank should be at a value greater than the fundamental structural frequency in order to gain maximum effectiveness under large amplitude excitation. Lamb's equation may be used to estimate the tank frequency with a modified length parameter representing the wetted perimeter.
- Stiffness degrading structural systems under large excitation may benefit from tanks that are dynamically tuned, i.e. the systems would theoretically 'soften' together.

In this analysis, tanks with other angles of slope were not investigated. If the angle of 0° (box) is hardening, and the 30° angle is softening, then there is some angle in between which is neutral. The value of this angle is not currently known, and the implications of such a property are not well understood at this time.

CONCLUSIONS

The non-linear stiffness and damping model developed by Yu [8] was used to analyse a sloped-bottom tuned liquid damper. The results clearly illustrate a system that is described by a softening spring. The primary benefit derived from the sloped-bottom tank is the reduction in beating; therefore, the practical application of these tanks indicate that the tank frequency should be at a frequency slightly higher than the fundamental natural frequency of the structure for maximum effectiveness. Further, the appropriate use of ' L ' in Lamb's equation provide a fairly close estimate of the tank natural frequency if empirical results are not readily available.

ACKNOWLEDGEMENTS

Suggestions by Prof. Harry Yeh of the University of Washington and Dr Jin-kyu Yu of Skilling, Ward, Magnusson, Barkshire, Inc. are gratefully acknowledged.

REFERENCES

1. Gardarsson S. Shallow-water sloshing. *Ph.D. Thesis*. University of Washington, Department of Civil Engineering, Seattle, WA, 98195, 160pp, 1997.
2. Gardarsson S, Yeh H, Reed DA. The behaviour of sloped-bottom tuned liquid dampers. *Journal of Engineering Mechanics* 2001, to appear.
3. Lepelletier TG, Raichlen F. Nonlinear oscillations in rectangular tanks. *Journal of Engineering Mechanics ASCE* 1988; **114**:1–23.
4. Chaiseri P, Fujino Y, Pacheco BM, Sun LM. Interaction of tuned liquid damper (TLD) and structure—theory, experimental verification and application. *Structural Engineering/Earthquake Engineering JSCE* 1989; **6**:273–282. (*Proceedings of JSCE* no. 410/1-12).

5. Fujino Y, Sun L, Pacheco BM, Chaiseri P. Tuned Liquid Damper (TLD) for Suppressing Horizontal Motion of Structures. *Journal of Engineering Mechanics* 1992; **118**:2017–2030.
6. Tamura Y, Kousaka R, Modi VJ. Practical application of nutation damper for suppressing wind-induced vibrations of airport towers. *Journal of Wind Engineering and Industrial Aerodynamics* 1992; **41/44**:1919–1930.
7. Zhao Z, Fujino Y. Numerical simulation and experimental study of deeper-water TLD in the presence of screens. *Journal of Structural Engineering JSCE* 1993; **39**:699–711.
8. Yu Jin-kyu. *Nonlinear characteristics of tuned liquid dampers*, Ph.D. Thesis, University of Washington, Department of Civil Engineering, Seattle, WA, 98195, 1997.
9. Lamb H. *Hydrodynamics* (6th edn). Cambridge University Press: Cambridge, 1932; 619–621.
10. Reed DA. Structural control using tuned liquid dampers. *Proceedings of the UJNR Workshop on Wind effects*, University of Hawaii at Manoa, Honolulu, Hawaii, 7–9 October, 1997.
11. Reed DA, Yeh H, Yu J, Gardarsson S. Experimental investigation of tuned liquid dampers. *Proceedings of the ASCE 1996 International Conference on Natural Disaster Reduction*, Washington, DC, December 1996.
12. Reed DA, Yeh H, Yu J, Gardarsson S. Performance of tuned liquid dampers for large amplitude excitation. *Proceedings of the Second International Workshop on Structural Control*, Hong Kong, December 1996.
13. Reed DA, Yu J, Yeh H, Gardarsson S. Investigation of tuned liquid dampers under large amplitude excitation. *Journal of Engineering Mechanics* 1998; **124**:405–413.
14. Sun LM, Fujino Y, Chaiseri P, Pacheco BM. The properties of tuned liquid dampers using TMD analogy. *Earthquake Engineering and Structural Dynamics* 1995; **24**:967–976.
15. Yalla S, Kareem A. Modelling tuned liquid dampers as sloshing–slamming dampers. *Wind Engineering into the 21st Century: Proceedings of the 10th International Conference on Wind Engineering*, Copenhagen, Denmark, June, 1999; 1569–1575.
16. Yu Jin-kyu, Wakahara T, Reed DA. A nonlinear numerical model of the tuned liquid damper. *Earthquake Engineering and Structural Dynamics* 1999; **28**:671–686.
17. Fujino Y, Pacheco BM, Chaiseri P, Sun L-M, Koga K. Understanding of TLD properties based on TMD Analogy. *Journal of Structural Engineering* 1990; **36A**:577–590 in (Japanese).
18. Koh CG, Mahatma S, Wang CM. Theoretical and experimental studies on rectangular liquid dampers under arbitrary excitations. *Earthquake Engineering and Structural Dynamics* 1994; **23**:17–31.

